

# Magnetic Living Hydrogels for Intestinal Localization, Retention, and Diagnosis

Xinyue Liu, Yueying Yang, Maria Eugenia Inda, Shaoting Lin, Jingjing Wu, Yoonho Kim, Xiaoyu Chen, Dacheng Ma, Timothy K. Lu,\* and Xuanhe Zhao\*

Natural microbial sensing circuits can be rewired into new gene networks to build living sensors that detect and respond to disease-associated biomolecules. However, synthetic living sensors, once ingested, are cleared from the gastrointestinal (GI) tract within 48 h; retaining devices in the intestinal lumen is prone to intestinal blockage or device migration. To localize synthetic microbes and safely extend their residence in the GI tract for health monitoring and sustained drug release, an ingestible magnetic hydrogel carrier is developed to transport diagnostic microbes to specific intestinal sites. The magnetic living hydrogel is localized and retained by attaching a magnet to the abdominal skin, resisting the peristaltic waves in the intestine. The device retention is validated in a human intestinal phantom and an in vivo rodent model, showing that the ingestible hydrogel maintains the integrated living bacteria for up to seven days, which allows the detection of heme for GI bleeding in the harsh environment of the gut. The retention of microelectronics is also demonstrated by incorporating a temperature sensor into the magnetic hydrogel carrier.

## 1. Introduction

Over the past few decades, technologies based on electronics and living bacteria have been developed for orally administered diagnostics and therapeutics.<sup>[1–8]</sup> The service life of existing

ingestible devices is limited by the gastrointestinal (GI) transit time, that is, the time it takes for food to move through the digestive system.<sup>[9,10]</sup> In the human body, the GI transit time usually ranges from 6 to 48 h.<sup>[2,11,12]</sup> However, for most GI applications, such as long-lasting biosignal collection,<sup>[9]</sup> prolonged drug delivery,<sup>[13,14]</sup> and sustained diet control,<sup>[15,16]</sup> longer retention times are needed. The effective diagnosis and treatment of GI diseases may also require ingestible devices to be positioned at a specific location in the gut. Such positioning would be desirable for the detection and treatment of localized diseases such as Crohn's disease, characterized by patchy inflammation along the GI tract.<sup>[17,18]</sup>

Although several strategies have been proposed to achieve localization in the GI tract, they all have limitations for intestinal

retention. For example, ingestible devices have been developed to reside in the GI tract by floating, unfolding, or swelling;<sup>[19,20]</sup> these can be applied to the large-volume gastric cavity but not to tubular structures (e.g., small and large intestines). There are high risks of intestinal blockage caused by the swelling hydrogels and of intestinal perforation caused by stiff or sharp pieces in the intestine.<sup>[2,9,21]</sup> Intestinal peristalsis may also induce the migration of unfolding structures, shortening their service life.<sup>[22]</sup> Moreover, intestinal mucus adhesion fails to anchor the materials and devices for more than four hours due to the rapid turnover of the mucus layer.<sup>[23–25]</sup> Finally, biological scaffolds that are continuously generated by engineered probiotics can persist in the intestine but may have side effects, including the irreversible alteration of the native gut microbiota.<sup>[26]</sup>


Magnetic materials have been of special interest for GI surgery because the magnetic force can be exerted over a distance.<sup>[27–29]</sup> Because of the constrained and tortuous architectures of the intestines, magnet-assisted spatial control is a useful feature for the diagnosis, evaluation, and management of localized pathologies, such as inflammation, ulcers, polyps, and tumors.<sup>[29,30]</sup> A number of magnet-assisted technologies have been utilized in the GI tract for spatial control, including the placement of enteral tubes,<sup>[31]</sup> the navigation of devices (e.g., capsule endoscopy and micromotors),<sup>[30,32]</sup> and the manipulation of surgical instruments (e.g., micro-snare, baskets, and forceps).<sup>[33]</sup> However, the existing surgical procedures require sophisticated medical equipment for spatial steering (e.g., X-ray

X. Liu, Y. Yang, Dr. S. Lin, Dr. J. Wu, Y. Kim, Dr. X. Chen, Prof. X. Zhao  
Department of Mechanical Engineering  
Massachusetts Institute of Technology  
Cambridge, MA 02139, USA  
E-mail: zhaox@mit.edu

Dr. M. E. Inda, Dr. D. Ma, Prof. T. K. Lu  
Synthetic Biology Group  
Research Laboratory of Electronics  
Massachusetts Institute of Technology  
Cambridge, MA 02139, USA  
E-mail: timlu@mit.edu

Dr. M. E. Inda, Dr. D. Ma, Prof. T. K. Lu  
Center for Biological Engineering  
Massachusetts Institute of Technology  
Cambridge, MA 02139, USA

Prof. X. Zhao  
Department of Civil and Environmental Engineering  
Massachusetts Institute of Technology  
Cambridge, MA 02139, USA

 The ORCID identification number(s) for the author(s) of this article can be found under <https://doi.org/10.1002/adfm.202010918>.

DOI: 10.1002/adfm.202010918

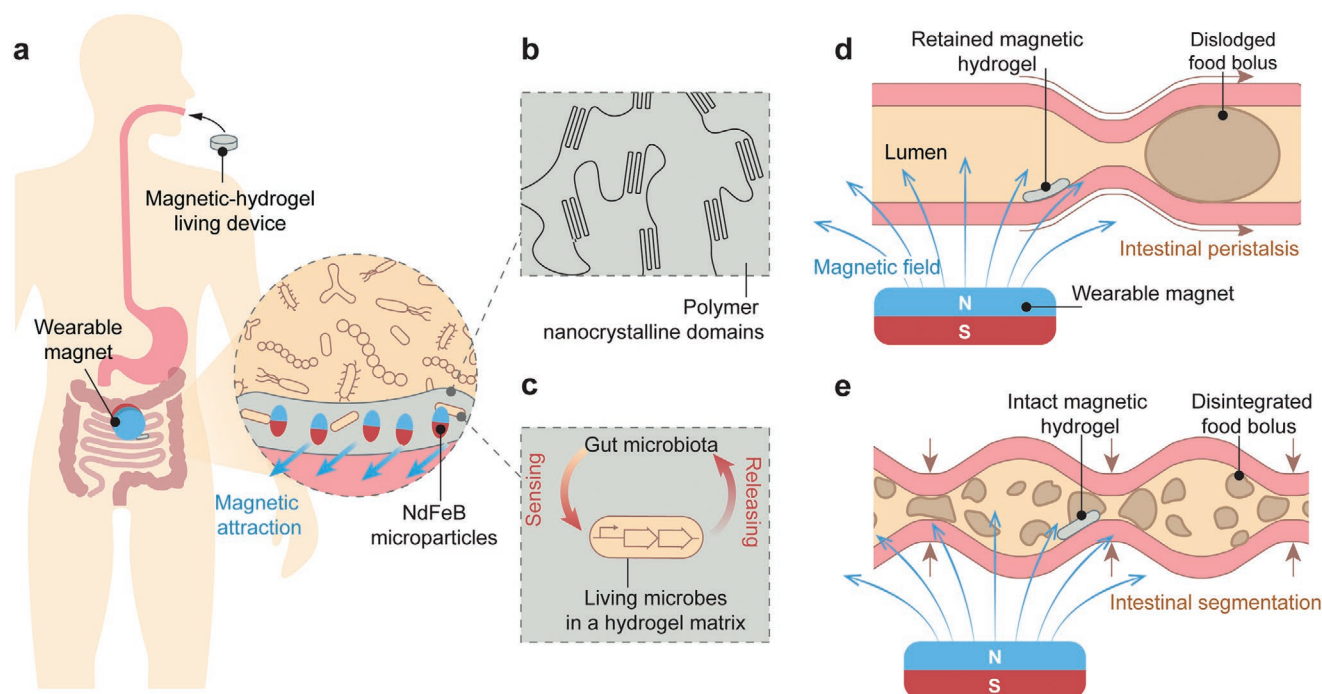


**Figure 1.** Design and mechanism of the magnetic living hydrogels localized and retained in the intestine. a) The magnetic living hydrogel is orally administrated and retained in the intestine by a magnet worn on the abdominal skin. Inset: magnetized NdFeB microparticles incorporated in the hydrogel matrix provide the attractive magnetic force between the magnetic hydrogel and wearable magnet for intestinal localization and retention. b) The hydrogel matrix is physically crosslinked by nanocrystalline domains and reinforced by NdFeB microparticles, making it mechanically tough. c) Living synthetic microbes encapsulated in the hydrogel matrix interact with the gut microbiota when the magnetic hydrogel is retained in the gut, enabling biological functions such as sensing and releasing. d) Intestinal peristalsis propels a food bolus along the intestinal lumen, while the magnetic hydrogel can be retained due to the magnetic attraction with the wearable magnet. e) Intestinal segmentation breaks a food bolus into fragments in the intestinal lumen, while the magnetic hydrogel can remain intact due to its mechanical toughness.

emitter, detector, and robotic arm), and subjects under anesthesia.<sup>[31–34]</sup> They are applicable only for temporary use because the surgical interventions prevent the free movement of the subjects. In order to have prolonged control over the magnetic materials in the GI tract and permit normal movement of the subject in daily life, we designed a wearable magnet that can allow both spatial localization and temporal retention of ingested magnetic materials.

Here, we built a magnetic hydrogel retentive system, consisting of an ingestible, magnetic hydrogel carrying diagnostic microbes that could be localized by a wearable neodymium magnet, for long-term disease diagnosis in the intestine (Figure 1a). To prevent dislocation of the magnetic living hydrogel due to peristaltic waves and intestinal fluid flow, we optimized attractive magnetic force between the magnetic hydrogel in the intestine and the magnet by tuning the magnet dimensions (Figure 1d). Since the ingestible hydrogel is soft and flexible, it conforms to the intestinal surface, minimizing tissue damage to the intestinal lining. The mechanical robustness of the ingestible hydrogel helps maintain its structural integrity during intestinal segmentation (Figure 1e). The wearable magnet is lightweight and portable, and causes minimal tissue compression. Most importantly, the magnetic hydrogel is sufficiently retained by the wearable magnet in both rodent and human models based on our theoretical calculation. We validated the capability of magnet-assisted retention and localization in a human-scale GI tract phantom and in free-moving

rodents (for at least a week) without causing any obstruction. Because the ingestible hydrogels are biocompatible, the living bacteria integrated into the soft hydrogel matrix were functional for 7 days in vitro (Figure 1c). Experimentally induced bleeding was detected by these biosensing bacteria in the mouse intestine. In contrast to other systems (e.g., magnetically driven position control) which require high-precision medical equipment and comprehensive procedures, the magnetic living hydrogel permits the prolonged monitoring and modulation of the digestive system and adjacent organs and constitutes a non-invasive, accessible platform for the intestinal localization and retention of bacterial biosensors and electronic sensors.

## 2. Results and Discussion

### 2.1. Design and Fabrication of Magnetic Living Hydrogels

Neodymium-iron-boron (NdFeB) magnets are hard ferromagnets that can retain high remanent magnetization after being magnetized.<sup>[28]</sup> Magnetic hydrogels for oral administration and intestinal retention were fabricated by incorporating NdFeB microparticles into a polyvinyl alcohol (PVA) hydrogel matrix (Figure 1a,b). First, these NdFeB microparticles (5  $\mu\text{m}$  in average diameter) were coated with a nanolayer of silica shell (10 nm in thickness) to protect the alloys from corrosion in the hydrated environment.<sup>[28]</sup> Overnight cultures of engineered

bacteria were centrifuged and resuspended in an equal volume of 10 wt% PVA solution. Then, NdFeB microparticles with volume fractions ranging from 0% to 21% were mixed with the bacteria-containing PVA solution and poured into a mold. The mixture in the mold was subjected to a strong impulse magnetic field (2.5 T) to magnetize the NdFeB microparticles along the applied field direction. This step of magnetization generated a uniform magnetic moment across the bulk mixture.<sup>[27]</sup> The PVA-NdFeB-bacteria mixture in the mold was then exposed to the temperature of  $-20\text{ }^{\circ}\text{C}$  for 24 h, which promotes the phase separation of polymers in water and the formation of nanocrystalline domains in the PVA solution, resulting in a hydrogel matrix (Figure 1b).<sup>[35]</sup>

The magnetic hydrogels are crosslinked by PVA nanocrystalline domains.<sup>[35,36]</sup> Increasing the volume fraction of NdFeB microparticles in the nanocrystalline hydrogel further contributes to a higher Young's modulus (Figure S1a, Supporting Information), higher toughness (Figure S1b, Supporting Information), and higher magnetization (Figure S1e, Supporting Information) of the magnetic hydrogel. We determined the amount of NdFeB microparticles in the magnetic hydrogel to be 12 vol%. The hydrogel with 12 vol% NdFeB exhibits a low Young's modulus of 21 kPa, a high toughness of  $\approx 280\text{ kJ m}^{-3}$ , and a high magnetization of  $6 \times 10^4\text{ A m}^{-1}$  (Figure S1a–e, Supporting Information). The low Young's modulus of the magnetic hydrogel drastically alleviates the stress concentration on the intestinal wall, as manifested by the finite element simulations (Figure S2d,e, Supporting Information). Low mechanical stiffness of hydrogels is also indispensable for maintaining the viability of encapsulated bacteria, especially in the long-term (Figure S3, Supporting Information). The high toughness of the magnetic hydrogel ensures the structural integrity when the hydrogel is subject to intestinal peristalsis and segmentation (Figure 1d,e). In addition, the high magnetization enables effective retention of the hydrogel and its localization in spite of intestinal motility (Figure S1e, Supporting Information).

## 2.2. Model for Retention of Magnetic Hydrogels

A large wearable magnet can produce a strong magnetic field favorable for the retention and localization of magnetic hydrogels, but may cause a series of side effects including tissue damage due to the magnetic attraction force and overload caused by a heavy magnet being worn on the body. We developed a model to rationally select the wearable magnet with optimized dimensions. The model included a disc-shaped wearable magnet and a disc-shaped magnetic hydrogel residing in a lumen with intestinal peristalsis (Figure 2a). The intestinal peristalsis in the lumen propels the hydrogel to move forward, and the friction between the hydrogel and the lumen wall resists the hydrogel's motion (Figure 2a,b). The intestinal propelling force is denoted as  $F^{\text{propel}}$ , and the friction force as  $F^{\text{friction}}$ . The magnetic force between the wearable magnet and the NdFeB microparticles in the hydrogel may propel or retain the magnetic hydrogel, depending on the direction of the magnetic force (Figure 2b).

We defined a cylindrical coordinate system with the center of the disc-shaped wearable magnet as the origin  $O$ , the radial

direction of the magnet as the  $r$ -axis, and the axial direction of the magnet as the  $z$ -axis (Figure 2a). In addition, the point  $P(r, z, \theta)$  refers to the center of the magnetic hydrogel, where  $\theta$  is the angle between the intestinal propelling direction and the projection of OP line segment on the upper surface of the magnet. (Figure 2a). We next calculated the magnetic force applied on the magnetic hydrogel. The magnetic field  $\mathbf{B}$  around the disc-shaped wearable magnet can be expressed as  $\mathbf{B} = B_r \mathbf{e}_r + B_z \mathbf{e}_z$ , where  $\mathbf{e}_r$  and  $\mathbf{e}_z$  are unit vectors in the direction of the  $r$ -axis and  $z$ -axis, respectively, and  $B_r$  and  $B_z$  are expressed in Supporting Information.<sup>[37]</sup> The axial direction of the disc-shaped magnetic hydrogel is assumed to be parallel with the axial direction of the wearable magnet. The vertical distance between the adjacent surfaces of the magnet and the hydrogel is  $D$ . The magnetic hydrogel is assumed to be uniformly magnetized with the remanent magnetization  $\mathbf{M}_h$  formed along the axial direction of the hydrogel (Figure 2b). We also assumed that the magnetization of the magnetic hydrogel is unaffected by the applied magnetic field  $\mathbf{B}$  due to the high coercivity of the NdFeB microparticles in the hydrogel.<sup>[28]</sup> Given the magnetic field applied by the magnet and the magnetization of the hydrogel, we calculated the magnetic force applied on the hydrogel as

$$\mathbf{F}^{\text{magnetic}} = \nabla \int_0^V \mathbf{M}_h \cdot \mathbf{B} dv \quad (1)$$

where  $V$  is the volume of the hydrogel and  $\nabla = \frac{\partial}{\partial r} \mathbf{e}_r + \frac{\partial}{\partial z} \mathbf{e}_z$ . Specifically, the magnetic force acting on the hydrogel can be decomposed into the force component along the  $z$  direction  $F_z$  and the force component along the  $r$  direction  $F_r$ , namely,  $\mathbf{F}^{\text{magnetic}} = -F_r \mathbf{e}_r - F_z \mathbf{e}_z$ , where  $F_r$  and  $F_z$  are both positive because the magnetic force is attractive between the magnet and the hydrogel (Figure 2b). The hydrogel can be effectively retained if the forces along  $r$  direction satisfy the criterion:

$$F^{\text{friction}} + F_r \cos \theta - F^{\text{propel}} \geq 0 \quad (2)$$

$\theta$  ranges from 0 to  $\pi/2$  when the magnetic hydrogel is on the downstream side of the magnet, and from  $\pi/2$  to  $\pi$  when the magnetic hydrogel is on the upstream side of the magnet (Figure 2a). In the current model, we further assumed the longitudinal axes of the lumen, the magnetic hydrogel, and the magnet are in the same plane, so that  $\theta = 0$  when the magnetic hydrogel is on the downstream side of the magnet, and  $\theta = \pi$  when the magnetic hydrogel is on the upstream side of the magnet (Figure 2a,b).

Based on the calculated intestinal propelling force, friction force, and magnetic force (see details in Supporting Information), we applied this criterion to a human model, where the vertical distance between the adjacent surfaces of the magnetic hydrogel and the magnet is 15 mm (Figure 2c). We fixed the thickness ( $L$ ) of the magnet to be 12.7 mm and varied its radius ( $a$ ) from 6.4 to 25.4 mm. We found that, when the radius of the magnet is greater than 9 mm, there exists a region in the lumen where the hydrogel can be retained. For example, when the radius of the magnet is 12.7 or 25.4 mm, the magnetic hydrogel can be successfully retained on the downstream side of the magnet (Figure 2c). The solid circles indicate the

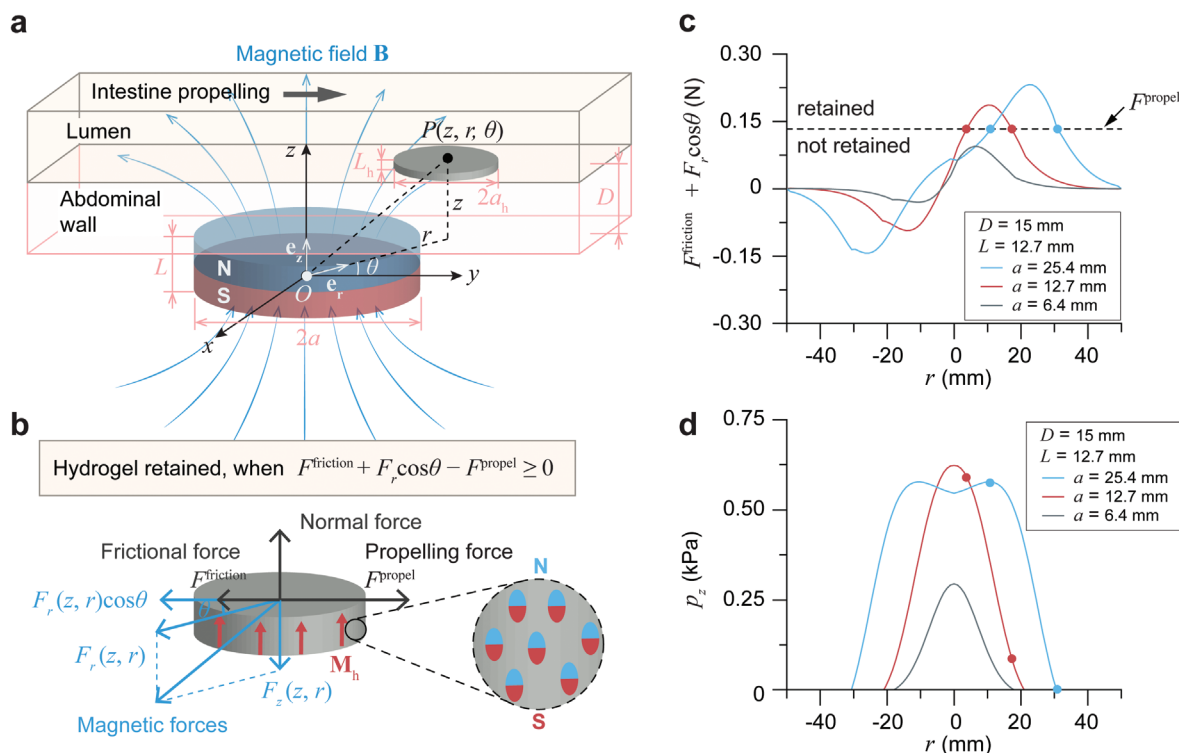


**Figure 2.** Model for intestinal retention and localization of the magnetic living hydrogel. a) Schematic illustration of a disc-shaped magnetic hydrogel (radius  $a_h$  and thickness  $L_h$ ) residing in a lumen under a magnetic field  $\mathbf{B}$  generated by a disc-shaped magnet (radius  $a$  and thickness  $L$ ). The vertical distance between the lumen and the magnet is  $D$ . b) Free body diagram of the magnetic hydrogel in the intestinal lumen, when it is moving along the intestinal propelling direction. The magnetization of the hydrogel  $\mathbf{M}_h$  is uniform and along the axial direction of the hydrogel disc. c) Net retarding force ( $F^{\text{friction}} + F_r \cos \theta$ ) of a magnetic hydrogel (radius  $a_h$  10 mm, thickness  $L_h$  1 mm) at a vertical distance of 15 mm away from a magnet (radius  $a$  6.4, 12.7, or 25.4 mm, thickness  $L$  12.7 mm). The magnetic hydrogel can be retained when the net retarding force is higher than the propelling force  $F^{\text{propel}}$ . d) Normal pressure  $p_z$  applied by a magnetic hydrogel (radius  $a_h$  10 mm, thickness  $L_h$  1 mm) on the intestinal wall at a vertical distance of 15 mm away from a magnet (radius  $a$  6.4, 12.7, or 25.4 mm, thickness  $L$  12.7 mm). Solid circles on each curve in (c, d) indicate the stably retained locations for the magnetic hydrogel, in which the retarding force ( $F^{\text{friction}} + F_r \cos \theta$ ) equals the propelling force  $F^{\text{propel}}$ .

stably retained locations for the magnetic hydrogels, at which  $F^{\text{friction}} + F_r \cos \theta - F^{\text{propel}} = 0$  with  $\theta = 0$ . To the contrary, the magnetic hydrogel can pass through the lumen without retention when the radius of the magnet is 6.4 mm (Figure 2c). In addition, as can be seen in Figure 2d, the normal pressure applied by the retained magnetic hydrogel on the intestinal wall is mild ( $p_z < 0.6$  kPa) at any retained locations around the magnets ( $a = 25.4$  or 12.7 mm,  $L = 12.7$  mm). Therefore, we selected the magnet with a radius of 25.4 mm and a thickness of 12.7 mm, due to the portable weight of the magnet (193 g), mild normal pressure applied on the intestinal tissue (0–0.6 kPa),<sup>[32]</sup> and capability of retaining the ingestible hydrogel (Figure 2c,d; Figure S4, Supporting Information).

### 2.3. In Vitro Retention of Magnetic Living Hydrogels

Next, we used transparent plastic tubes with flowing liquids to replicate the geometries and dimensions of mouse and human small intestines, and investigated the in vitro retention and positioning of magnetic living hydrogels based on remote magnetic attraction. In human intestines, the luminal chyme movement is driven by waves of contraction propagating along the intestinal wall.<sup>[38]</sup> To model the propelling force,

fluid flow at different flow rates and viscosities were generated in the tube by a peristaltic pump, which applied a shear stress of 0–10 kPa to the trapped contents close to the wall. As illustrated in Figure 3a,c, the fluid flow drove the motion of the suspended magnetic hydrogel so that it travelled through the whole conduit. In contrast, a magnet placed beneath the tube at a distance (2 mm for a mouse size and 15 mm for a human size) arrested the smooth movement of the magnetic hydrogel in the tube and kept the hydrogel static for 24 h afterward (Figure 3b,d; Video S1, Supporting Information). The magnetic force was able to resist a maximum shear stress of 10 kPa in tubes having the same size as the mouse or human small intestine (Figure 3e,f; Figure S5a and Video S1, Supporting Information). When the magnet was removed, the originally retained hydrogel moved forward through the tube (Figure S5b, Supporting Information).

To illustrate the potential utility of the magnetic hydrogel in the clinical setting, we examined the localization and retention of the ingestible magnetic hydrogel with a more clinically relevant model. We used a life-sized, silicone phantom that replicates the anatomy of human intestines, including the small and large intestine. As seen in Figure 3g, the tubular structure of the phantom is continuous and tortuous, containing several acute-angled corners, and its inlet and outlet



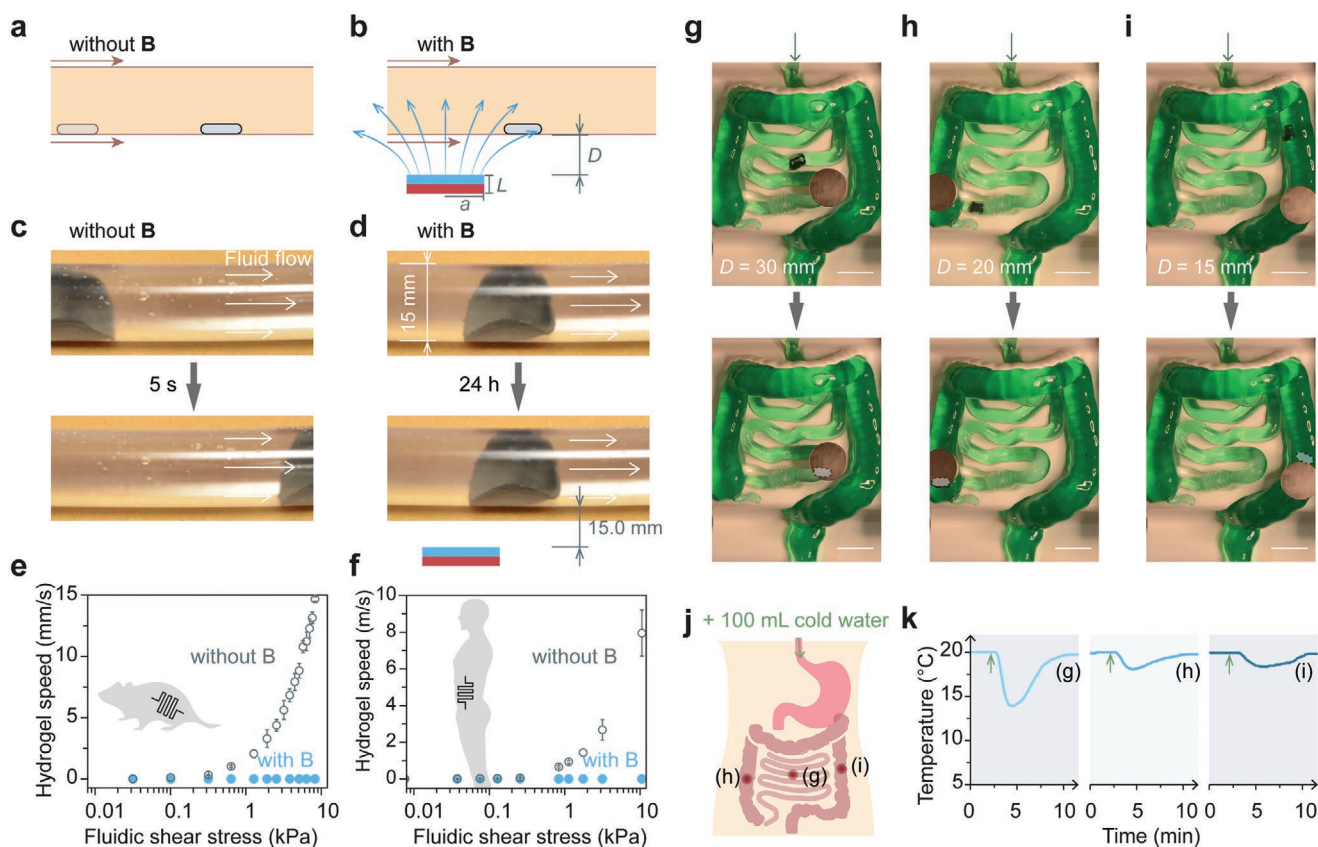


**Figure 3.** In vitro validation of retention and localization of the magnetic living hydrogel. a) Schematic illustration of the magnetic hydrogel movement propelled by intestinal peristalsis without any external magnet. Magnetic field, **B**. b) Schematic illustration of the magnetic hydrogel retention by the magnetic attraction force. c) Movement of a magnetic hydrogel (radius 10 mm, thickness 1 mm) in a transparent plastic tube (diameter 15 mm) driven by the fluidic flow without any external magnet. d) Retention of a magnetic hydrogel in a transparent plastic tube (diameter 15 mm) for 24 h with an external magnet (radius 25.4 mm, thickness 12.7 mm) placed 15 mm beneath the tube. e) Moving speed of a magnetic hydrogel (radius 1 mm, thickness 1 mm) against different fluidic shear stresses in a tube with dimensions similar to those of mouse intestines, with and without an external magnet (radius 5.6 mm, thickness 1.6 mm) at a vertical distance of 2 mm. f) Moving speed of a magnetic hydrogel (radius 10 mm, thickness 1 mm) against different fluidic shear stresses in a tube with dimensions similar to those of human intestines, with and without an external magnet (radius 25.4 mm, thickness 12.7 mm) at a vertical distance of 15 mm. g–i) Localization and retention of an integrated system consisting of a magnetic hydrogel (radius 10 mm, thickness 1 mm) and a miniature temperature sensor in a silicone phantom mimicking the human intestine, and the integrated system was pinned at the g) small intestine, h) ascending colon, and i) descending colon by an external magnet (radius 25.4 mm, thickness 12.7 mm) placed 15–30 mm above the phantom. Scale bars in (g–i): 50 mm. j) Schematic illustration of oral intake of cold water to the GI tract and three locations (g–i) where the temperature was probed after water intake. k) Temperature variations after cold water intake measured by a miniature temperature sensor when the integrated system was retained at the three locations in the GI tract.

are connected to a peristaltic pump with a flow flux of  $3400 \text{ mL min}^{-1}$ . The magnetic hydrogel alone automatically passed through the artificial intestine without any navigation (Figure S6a and Video S2, Supporting Information). When a magnet was placed on a transparent acrylic sheet right above the winding intestine phantom (distance 15–30 mm), the magnetic hydrogel was retained at several different locations, such as the small intestine, ascending colon, and descending colon (Figure S6b and Video S3, Supporting Information). When the magnetic hydrogel encapsulated a miniature temperature sensor (6 mm in diameter and 17 mm in length), the hydrogel piece was effectively pinned by the magnet placed above at several different locations corresponding to the small intestine (Figure 3g), the ascending colon (Figure 3h), and the descending colon (Figure 3i) in the phantom. Since the overall diameter of the electronic sensor-encapsulated

magnetic hydrogel was around 8 mm, smaller than the inner diameters of artificial intestines (15 mm for small intestine, 20–43 mm for large intestine), it did not obstruct fluid flow. Furthermore, the strong static magnetic field imposed by the wearable magnet did not affect the temperature sensing and recording functions of the microelectronics. When we infused 100 mL of cold water ( $0^\circ\text{C}$ ) through the inlet of the tubular phantom to replicate water drinking, temperature variations at different locations were recorded (points (g–h) in Figure 3j). Figure 3k indicates that the intake of cold drinks induced temperature variations, and the magnitude and delay time of these variations depended on the locations in the GI tract. When the integrated sensor was close to the inlet (g), the temperature decrease was swift and sharp, whereas there were gradual and gentle temperature fluctuations in the downstream regions, as seen in (h) and (i).

## 2.4. In Vitro Biocompatibility of Magnetic Living Hydrogels

Interfacing magnetic hydrogels with the human body requires assessments of chemical corrosion and cytotoxicity. We further investigated the corrosion of embedded NdFeB alloys in magnetic hydrogels by element analysis of the leaching solution. The as-prepared magnetic hydrogels were incubated in simulated gastric fluids (pH 1.2) at 37 °C for 1 day and simulated intestinal fluids (pH 6.8) at 37 °C for 10 days to allow the solvent to extract corroded metal ions, including Nd(III) and Fe(III). Element concentrations in these aqueous solutions were obtained by inductively coupled plasma mass spectrometry, from which we calculated the quantity of neodymium and iron ions that were corroded and dissolved from 1 g of magnetic hydrogel in 1 mL of fluids. The lower limits of toxicity, calculated by oral LD50 (i.e., 0.2 g kg<sup>-1</sup> for FeCl<sub>3</sub> and 3.7 g kg<sup>-1</sup> for NdCl<sub>3</sub>) times an average human weight (i.e., 62 kg), were orders of magnitude higher than the amounts of corroded ions [Nd(III) and Fe(III)] from 1 g of magnetic hydrogel over 10 days (Figure 4a), suggesting that the presence of silica shells on the NdFeB particles would help to minimize direct exposure of the alloys to intestinal environments with neutral pH and consequently limit corrosion. The magnetic hydrogels were more severely oxidized and corroded in acidic solution, when they were incubated with simulated gastric fluid (pH 1.2) for 4 h, but the concentrations of corroded metal ions were still much lower than the limits of oral doses that induce toxicity (Figure 4a).

We then analyzed the cytotoxicity of magnetic hydrogels using the Caco-2 cell line, which has been widely used as a model of the epithelial barrier on the intestine.<sup>[39]</sup> Similar to the trace element analysis mentioned above, leaching experiments were used to collect the chemicals released from magnetic hydrogels in fresh culture media for 1–7 days. Caco-2 cells were then exposed to the culture media containing the released compounds and left for 2 days, and cell viability was analyzed by using live/dead cell stains. As shown in Figure 4b,c and Figure S7, Supporting Information, there was no significant difference in viability for cells kept in the pristine culture medium (positive control), and the media that had been exposed to the magnetic hydrogels and pure PVA hydrogels for 1–7 days.

To determine whether the magnetic hydrogels could maintain living bacteria, as well as to test their in vitro functionality, we used a strain of engineered *Escherichia coli* (*E. coli*) Nissle 1917 as a bacterial blood sensor. These probiotic bacteria have been genetically engineered with the gene of P<sub>L(HrtR)</sub>-*luxCDABE* with HrtR.<sup>[12]</sup> When they are physically entrapped in the magnetic hydrogel, they express bioluminescence when extracellular heme is present in the surrounding medium. As demonstrated in Figure 4d,e, bacterial viability in the hydrogel was maintained above 95% for a week after day 0, and the colony size and density of viable bacteria continuously grew post-encapsulation. A few factors contributed to this lasting survival and growth: the biocompatibility of the chemical components and the fabrication process; chemical permeability, which allowed mass transport of nutrient supplies and metabolic products (Figure S1f, Supporting Information); and mechanical softness, which permitted bacterial growth and division within the hydrogel matrix (Figure 4f; Figure S3, Supporting Information).<sup>[40,41]</sup> We then validated the biosensing function of the bacteria encapsulated

in the magnetic hydrogels. As shown in Figure 4g, visible luminescence production in the hydrogels was induced by 0.1 vol% of whole horse blood in vitro. The induction tests were conducted at different time points of hydrogel incubation, during which the normalized luminescence gradually decreased from 33 after 24-h incubation to 7.5 after 7 days (Figure 4g).

## 2.5. In Vivo Retention and Sensing Ability of Magnetic Living Hydrogels

After establishing the retention and positioning of the magnetic hydrogel in vitro, we evaluated the in vivo intestinal retentive ability of magnetic hydrogels in a mouse model (C57BL/6, Jackson Laboratory). Despite differences in size and physiology with the human body, mouse models have been frequently adopted to study the gut microbiota and the interactions of gut microbes with the host; in fact, mice share a similar GI transit time with humans.<sup>[42,43]</sup> Magnetic living hydrogels (radius 1 mm, thickness 1 mm) were dispersed in a block of nutritious jelly (DietGel 76A, ClearH<sub>2</sub>O) and provided to mice after overnight fasting, so that mice would voluntarily consume the DietGel together with the magnetic hydrogels through oral administration without gavage or other invasive procedures (Figure S8, Supporting Information). Owing to high radiographic contrast between magnetic hydrogels and mouse tissues, we employed X-ray microtomography (microCT) to visualize the 3D spatial position of the magnetic hydrogels in the GI tract over time. We observed that fasted mice ingested the magnetic hydrogels within approximately one hour after DietGel distribution. Mice with ingested magnetic hydrogels inside their bodies were randomly allocated into two groups: the control group without any treatment (*n* = 5) and the experimental group carrying a disc-shaped magnet (radius 11 mm, thickness 1.6 mm), which was adhered on the abdomen by skin adhesives (*n* = 5).

As illustrated in Figure 5a,c, the ingested magnetic hydrogel was completely cleared from the GI tract in the control group within 6 h. The magnetic hydrogel, in contrast, was magnetically retained in the GI tract for 7 days in the experimental group (Figure 5b,d; Video S4, Supporting Information). After the removal of the magnet from the abdomen, the magnetic hydrogel was released rapidly and completed its passage through the remaining tract within 6 h (Figure S8 and Video S5, Supporting Information). During its retention period, the magnetic hydrogel was able to resist the mechanical loads caused by intestinal motility and preserve its structural integrity. As indicated in the representative histological images of the small intestine cross-section with (Figure 5f) and without (Figure 5e) a magnetic hydrogel, intestinal tissues in contact with the magnetic hydrogel did not exhibit significant inflammatory responses, nor was the intestinal lumen blocked by the retained hydrogel. In addition, although the extracorporeal magnet exerted robust magnetic control of the ingestible hydrogel, no significant change in overall animal well-being, including body weight, movement, and food/water intake, was observed in the animals.

To demonstrate that magnetic hydrogels can serve as universal carriers for living sensors in vivo, we verified the biomarker detection in mice enabled by living bacteria

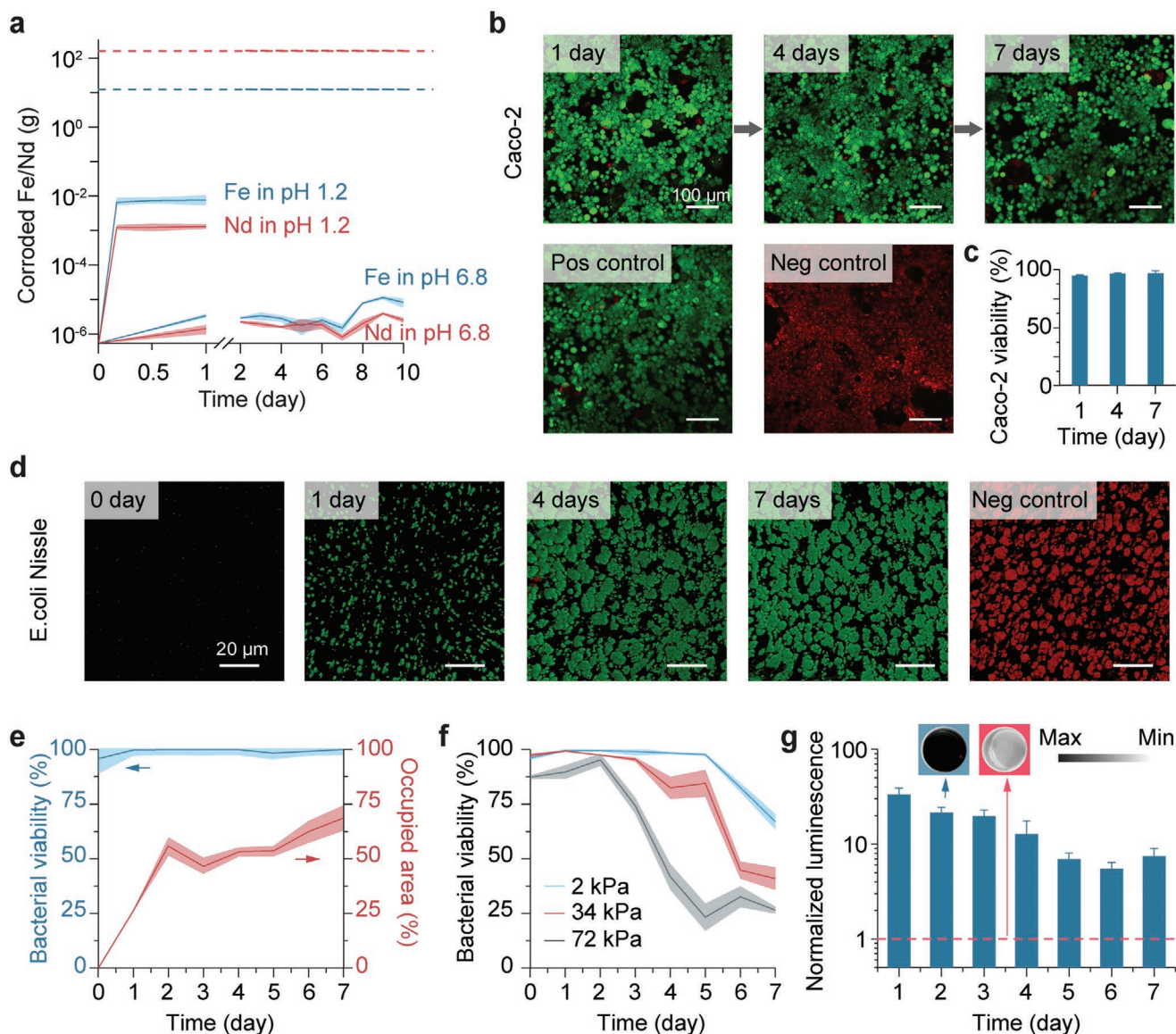


**Figure 4.** Biocompatibility and functionality of the magnetic living hydrogel. a) Chemical element analysis of the corroded metal ions from the magnetic hydrogel in simulated gastric fluid (pH 1.2) over 24 h and in simulated intestinal fluid (pH 6.8) over 10 days. The values correspond to the corroded metal masses from 1 g of the magnetic hydrogel, and represent the mean  $\pm$  s.d. ( $n = 4$ ). Dashed lines represent maximum oral doses having no significant toxic effect. b) Biocompatibility of the magnetic hydrogel in a live/dead assay of Caco-2 cells, using a hydrogel-conditioned medium (conditioning time: 1, 4, 7 days) for cell culture. After culture, the Caco-2 cells were stained with calcein-AM (green) and ethidium homodimer-1 (red) to visualize the viable and dead cells, respectively. Scale bars: 100  $\mu\text{m}$ . c) Caco-2 cell viability using a hydrogel-conditioned medium with varied conditioning time. The values represent the mean  $\pm$  s.d. ( $n = 3$ ). d) Encapsulation and visualization of engineered bacteria (*E. coli* Nissle 1917) in the magnetic hydrogel for 1–7 days. The encapsulated bacteria were stained with SYTO 9 dye (green) and propidium iodide (red) to visualize the viable and dead bacteria, respectively. Scale bars: 20  $\mu\text{m}$ . e) Bacterial viability and area occupied by viable bacteria (*E. coli* Nissle 1917) in hydrogels over time. The values represent the mean  $\pm$  s.d. ( $n = 3$ ). f) Bacterial viability (*E. coli* DH5 $\alpha$ ) in hydrogels with varied Young's modulus over time. The values represent the mean  $\pm$  s.d. ( $n = 3$ ). g) Blood-sensing ability of the magnetic living hydrogels that encapsulated engineered bacteria. The values represent the mean  $\pm$  s.d. ( $n = 3$ ). Insets: typical images of the luminescent hydrogel (left, blue background) and non-luminescent hydrogel (right, red background; negative control). Dashed red line represents values obtained with the negative control.

encapsulated in the intestinal retentive hydrogel. We chose *E. coli* Nissle 1917 as a chassis for its excellent safety profile for long-term use and its incapacity to colonize the gut if swallowed.<sup>[44]</sup> Direct oral administration of *E. coli* Nissle 1917 resulted in viable cells in stools on the first day of administration (peak at the 6th hour), but bacteria were completely cleared in the subjects afterward.<sup>[12,44]</sup> In general, the delivery

of bacteria to the small intestine is challenging: colonization by the bacteria of the gut microbiota may cause drastic microbiome perturbation; while competition for nutrients and location with resident microbes may prevent the engrafted bacteria from colonizing, so that they lose their efficacy.<sup>[45]</sup> Constraining the location of the engineered bacteria by encapsulating them in the magnetic hydrogel offers a solution, because it not only



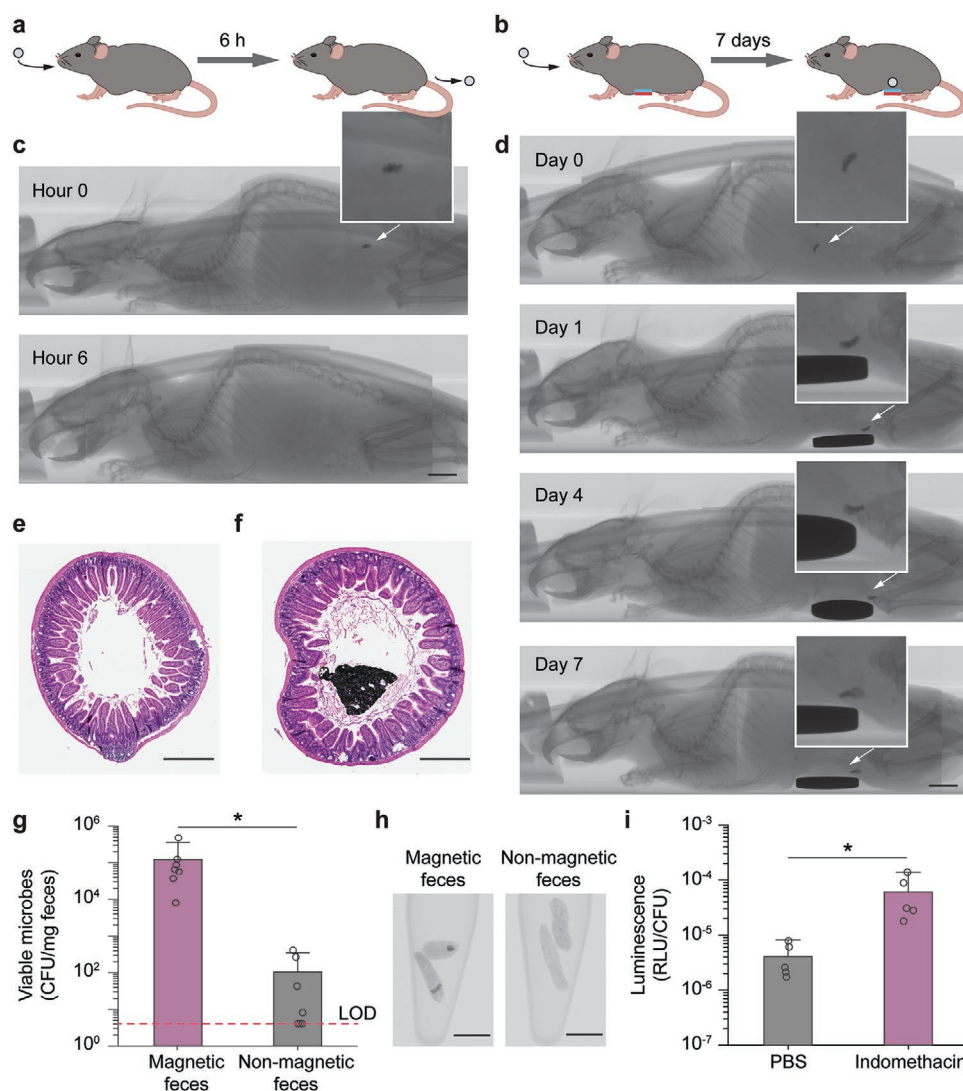


**Figure 5.** In vivo validation of magnet-assisted retention and in vivo heme sensing function of the magnetic living hydrogels. a) Illustration of an ingested magnetic living hydrogel passing through the whole GI tract of a mouse within  $\approx 6$  h. b) Illustration of an ingested magnetic living hydrogel retained in the GI tract of a mouse for 7 days by an external magnet attached to the abdomen. c) CT images of a mouse with an ingested magnetic living hydrogel passing through the whole GI tract of a mouse within  $\approx 6$  h. d) CT images of a mouse with an ingested magnetic living hydrogel retained in its intestine for 7 days by an extracorporeal magnet attached on the abdomen. Scale bars in (c,d): 5 mm. e,f) Representative histological images stained with haematoxylin and eosin (H&E) for assessment of the small intestine cross-section without (e) and with (f) a magnetic hydrogel after 7-day intestinal retention. Scale bars: 500  $\mu\text{m}$ . g) Numbers of viable microbes in fecal pellets collected from mice at 12 h post-administration of the hydrogel (containing blood-sensing *E. coli* Nissle 1917). The fecal samples with and without magnetic hydrogels exhibit significant differences in microbe numbers ( $*p < 0.05$ ; Student's *t*-test;  $n = 7$ ). Dashed line indicates the limit of detection (LOD) of the assay. h) CT images of fecal pellets with or without magnetic hydrogels. Scale bars: 5 mm. i) In vivo blood sensing performance. After the magnetic hydrogel (containing blood-sensing *E. coli* Nissle 1917) was retained in the intestine, mice were administered indomethacin (to induce gastrointestinal bleeding) or PBS. Normalized luminescence values of fecal pellets 24 h post-induction are significantly higher in mice administered indomethacin compared to control animals ( $*p < 0.05$ ; Student's *t*-test;  $n = 5$ ). RLU, relative luminescence units.

allows long-term, localized residence of bacteria in the GI tract to overcome resistance to colonization but also reduces undesirable dispersion of the gut microbiota. We first fed the animals with the bacteria-encapsulating magnetic hydrogels. After 12 h, we removed the magnet discs on the abdomen. Then, 1–6 h after magnet removal, microbes were recovered from the stool samples. In the collected feces with no magnetic hydrogel, few viable bacteria ( $0\text{--}10^3$  CFU  $\text{mg}^{-1}$  feces, CFU, colony-forming units) were detected (Figure 5g,h). In contrast,

there were  $\approx 10^5$  CFU of bacteria in 1 mg of fecal samples containing magnetic hydrogels (Figure 5g,h). The difference in numbers of living bacteria recovered from collected fecal samples with and without magnetic hydrogels indicated that the hydrogel-encapsulated bacteria were contained in the hydrogel without significant alteration of the global gut microbiota. It also showed that high loads of bacteria can be retained, which would be useful for efficient therapeutic delivery and accurate biosensing.



To determine whether this system was responsive to GI bleeding elicited by indomethacin, we tested the bacterial blood sensor encapsulated in the ingested magnetic hydrogels. C57BL/6J mice carrying the magnetic living hydrogels were administered indomethacin (10 mg kg<sup>-1</sup>) to induce GI bleeding in the experimental group ( $n = 5$ ) and phosphate-buffered saline (PBS) in controls ( $n = 5$ ). Twenty-four hours after indomethacin administration in the experimental group, the magnets on the abdomen were removed and fecal pellets in both groups were collected. We performed the CT scanning to confirm the presence of the magnetic hydrogels, luminescence analysis and CFU enumeration to calculate the bacterial luminescence, and guaiac test to validate the GI bleeding in the mice. As seen in Figure 5i, normalized luminescence values of fecal pellets were significantly higher in mice administered with indomethacin compared to those of control animals. The results revealed that the 24-h, localized colonization of the bacterial sensors in the mouse intestine allows effective detection of GI bleeding in vivo.

### 3. Conclusions

In summary, we introduced a magnetic hydrogel retentive system that combined an ingestible magnetic living hydrogel with a wearable magnet. This system relied on magnetic attraction to counteract the propelling effects of normal intestinal motility. Using theoretical calculations, we optimized the dimensions of the extracorporeal magnet for retention of the magnetic hydrogels applicable to either mice or humans. The retention and positioning of the magnetic hydrogel under the control of an extracorporeal magnet were verified by using a mouse-sized tube, a human-sized tube, a human-sized intestine phantom in vitro, and a mouse model in vivo. By incorporating genetically engineered heme-sensing bacteria into the ingestible hydrogel, we demonstrated that the device functioned to detect GI bleeding, as a proof of concept for biosensing in the gut. Engineering bacteria encapsulated in the protective magnetic hydrogel could thus perform diagnostic functions at localized sites in the gut.

The magnetic living hydrogels display a few advantages over other systems for tracking and treating conditions in the GI tract. The magnetic living materials are designed to have precise spatial localization, so their effects are also likely to be highly localized. When the hydrogel interacts with the intestinal tissues, alteration of the overall gut environment is likely to be minimized, because the bacteria are encapsulated. The mechanical flexibility and biological compatibility of the ingestible magnetic hydrogel minimized mechanical and biological mismatch between the tissue and the device. The tissue-like softness of the device is likely to prevent it from causing tissue injury. Intestinal obstruction is unlikely, because the device is much smaller than the diameter of the intestinal lumen. The magnetic living hydrogels have several additional advantages. Compared to laparotomy and laparoscopic surgery, these ingestible hydrogels are non-invasive. Furthermore, they do not rely on medical professionals with complicated equipment and procedures.<sup>[29,32,33]</sup> We expect that the remote control achieved by wearing an extracorporeal magnet and ingesting hydrogels can reduce cost (i.e., <\$50 for a set), simplify deployment (i.e.,

wearing and ingestion), and enable much wider applicability than the current methods,<sup>[32]</sup> which require patients to be anesthetized).

There is still room for improvement in the current magnetic hydrogel retentive system. First, the dimensional discrepancy between mouse and human may limit the generalization of the results obtained from mouse studies to clinical settings.<sup>[42]</sup> The distance between the two parts affects magnetic control: given that the magnetic field varies inversely with the third power of distance and that magnetic force varies inversely with the fourth power of distance,<sup>[28]</sup> validation in large animal species such as pigs and dogs will be required prior to translation to humans. Second, we have shown blood sensing and temperature recording in this work as a proof of concept to demonstrate several functionalities of the intestinal retentive hydrogels. Magnetic hydrogels can also be combined with other actuators, optics, or electronics<sup>[15,27]</sup> to enable a range of biomedical applications for these intestinal retentive devices. For example, coupling with bioelectronics to transduce the detected values in real-time<sup>[12]</sup> and wiring them to next-step actuation would achieve a series of semi-autonomous or autonomous programs while the device is retained in the intestine.<sup>[8,27]</sup> Ultimately, spatially localized and temporally retained hydrogel devices may be used to deliver drug-producing bacteria at targeted enteric sites, which can overcome the shortcomings of systemic treatment (e.g., frequent high-dose injections and side effects) and conventional oral administration (e.g., protein degradation in the acidic, protease-rich upper GI tract). Incorporating drug-producing bacteria in the intestinal retentive hydrogel could allow the requisite doses to be reduced by several orders of magnitudes, thus reducing systemic side effects.<sup>[46,47]</sup>

### 4. Experimental Section

**Bacterial Strains:** Plasmid construction and DNA manipulations of bacteria were performed following standard molecular biology techniques. Genetics parts and plasmids used in this study are available from Addgene and the previous paper.<sup>[12]</sup> All plasmids were constructed by combining PCR fragments generated by Kapa HiFi Polymerase using Gibson assembly.<sup>[12]</sup> Routine cloning and plasmid propagation were performed in *E. coli* DH5 $\alpha$ , and the gene circuits were transferred into probiotic *E. coli* Nissle 1917 for bacterial encapsulation.

**Fabrication of Magnetic Living Hydrogels:** NdFeB microparticles were coated with a thin shell of silica based on the condensation reaction of tetraethylorthosilicate (TEOS), which nucleated around the particles to form a cross-linked silica layer.<sup>[28]</sup> First, 40 g of NdFeB microparticles was dispersed in 1000 mL of ethanol with vigorously stirring to avoid sedimentation at 1500 rpm using a digital mixer (Cole-Parmer). Then, 60 mL of 29% ammonium hydroxide was slowly added to the mixture, followed by slow addition of 2 mL of TEOS. The mixture was stirred for 12 h at room temperature and then washed with acetone multiple times after the reaction. The suspension was then vacuum-filtered to obtain the silica-coated microparticles.

Engineered bacteria were routinely cultured overnight at 37 °C in Luria-Bertani (LB) media (Difco) supplemented with 50  $\mu$ g mL<sup>-1</sup> kanamycin. For bacterial encapsulation, overnight cultures of bacteria (*E. coli* Nissle 1917, 10 mL) were centrifuged at 5000  $\times$  g for 5 min, followed by supernatant removal. The remaining bacteria pellets were resuspended in 10 mL of 10 wt% PVA solution ( $M_w$  146 000–186 000, 99+% hydrolyzed, Sigma-Aldrich) using a planetary mixer (AR-100, Thinky) at 2000 rpm for 2 min. The magnetic hydrogel was prepared by homogeneously mixing silica-coated NdFeB microparticles with an average size of 5  $\mu$ m

(MQFP-B 20441-089, Magnequench) into the bacteria-containing PVA solution using a planetary mixer (AR-100, Thinky) at 2000 rpm for 2 min. The mixture was then magnetized by impulse magnetic fields (about 2.5 T) generated by an impulse magnetizer (IM-10-30, ASC Scientific) to impart magnetic polarities to the NdFeB microparticles embedded in the uncured PVA solution. Afterward, the magnetized solution was exposed to  $-20\text{ }^{\circ}\text{C}$  for 24 h, resulting in a physically crosslinked hydrogel matrix. Magnetic hydrogels with different Young's moduli in Figure 4f and Figure S3, Supporting Information, were fabricated by adjusting the freezing time from 2 to 48 h. Bacteria (*E. coli* DH5 $\alpha$ ) were encapsulated in the magnetic hydrogels with different Young's moduli.

**Mechanical Characterization:** Magnetic living hydrogels based on PVA and NdFeB with different particle concentrations were prepared and then swollen in phosphate-buffered saline (PBS) for 1 h. Subsequently, they were cut into dog bone shaped specimens with known dimensions (width 4.7 mm, thickness 1.6 mm, gauge length 17 mm) for tensile testing. The specimens were tested on a mechanical testing machine (Z2.5, Zwick/Roell) with a 20-N load cell at a strain rate of  $0.01\text{ s}^{-1}$ . A nominal stress–stretch curve was plotted for each specimen, and the Young's modulus and toughness were identified by the initial slope and the area under the stress–strain curve, respectively.

**Magnetic Characterization:** The magnetic moment densities of magnetic hydrogels based on PVA and NdFeB with different particle concentrations were measured with a vibrating sample magnetometer (DMS 1660, ADE Technologies). Specimens were prepared from thin sheets of the hydrogels obtained from molding by cutting them into 6-mm circles using a biopsy punch (size 6, Miltex) to fit into the sample holder of the magnetometer. The remanent magnetization of the samples was measured when the applied external magnetic field was zero and then divided by the sample volume to obtain the magnetization or magnetic moment density.

**Magnetic Field Measurement and Shielding:** An AC/DC magnetic meter (PCE-MFM 3000) was used to measure the magnitude of the magnetic field near the magnet (DY08-N52, K&J Magnetics). A sheet of spring steel (thickness 2.6 mm, McMaster Carr) was attached to the magnet for shielding the magnetic field.

**Diffusion Coefficient Measurement:** Diffusion coefficients of molecules within the magnetic hydrogels (12 vol% NdFeB) were determined using fluorescence recovery after photobleaching (FRAP). A series of fluorescent probes, that is, fluorescein isothiocyanate-dextran with molecular weights of 500 Da, 4 kDa, 10 kDa, and 70 kDa (FITC-dextran, Sigma-Aldrich) were dissolved in PBS at  $5\text{ mg mL}^{-1}$ . The magnetic hydrogels (1 g) were added to the fluorescent solution (50 mL), yielding a final concentration of  $5\text{ mg mL}^{-1}$  FITC-dextran in the hydrogels. FRAP measurement of diffusion coefficients was performed on a confocal microscope (SP 8, Leica) with a 5 $\times$  magnification objective and a 488 nm laser. A circle (radius  $\omega$  15  $\mu\text{m}$ ) was selected as the bleaching spot. Twenty pre-bleach images were scanned at a low laser intensity (1%), then the bleaching spot was bleached with five iterations ( $\approx 2.6\text{ s}$  in total) at 100% laser intensity, and followed by detection of the fluorescence recovery in the bleaching spot at low intensity (1%). For each experiment, a normalized fluorescence recovery curve and a fitting parameter, the characteristic diffusion time  $\tau_D$ , were obtained. The diffusion coefficient  $D_h$  was then calculated according to  $D_h = 0.22 \omega^2 / \tau_D$ .

**Friction Coefficient Measurement:** Magnetic hydrogel samples (20 mm  $\times$  20 mm  $\times$  1 mm) were prepared with 12 vol% NdFeB microparticles. To quantify the friction coefficients, the torque required to shear the specimens at a prescribed shear rate of  $1.0\text{ s}^{-1}$  under prescribed normal pressure (from 1.5 to 9 kPa) was measured from a rotational rheometer (AR-G2, TA Instruments) in normal force control mode with a 20-mm-diameter steel plate geometry. In the control group, deionized water was smeared between the hydrogel sample and steel plate before shearing the samples. In the experimental group, a piece of mucus-covered intestinal tissue (Sierra Medical Inc.) was attached to the steel plate and the mucus layer was brought in contact with the magnetic hydrogel. The friction coefficients were calculated following the previously reported protocol.<sup>[48]</sup>

**Retention in a Plastic Tube:** A transparent polyvinyl chloride tube (McMaster Carr) with the inner diameter of 2 mm or 15 mm was filled

with liquid (i.e., water,  $8.90 \times 10^{-4}\text{ Pa s}$  in viscosity; or glycerol, 1.4 Pa s in viscosity) and a magnetic hydrogel. Two ends of the plastic tube were then connected to a soft rubber tube (Masterflex L/S), which was loaded into a peristaltic pump (Masterflex L/S) to drive the fluid flow in the tube. A magnet (D71-N52 or DY08-N52, K&J Magnetics) was placed beneath the tube at a distance. The shear stress at the wall is written as  $\tau_w = \frac{4\eta Q}{\pi r_{\text{tube}}^3}$ , where  $\eta$  is the fluid viscosity,  $Q$  is the flow flux of the fluid, and  $r_{\text{tube}}$  is the radius of the tube.

**Retention and Localization in a Silicone Phantom:** An intestine phantom model made of silicone (Trandomed 3D) was custom-designed and 3D-printed. This silicone phantom was filled with swollen polyacrylate particles (Waste Lock 770, M2 Polymer) and connected to a peristaltic pump (Masterflex L/S) to simulate the intestinal peristalsis. In the set of demonstrations, the retention and localization were controlled by a magnet (DY08-N52, K&J Magnetics) on a transparent acrylic sheet which was placed horizontally on top of the phantom at a closest distance of 15 mm.

**Temperature Sensing in a Silicone Phantom:** The magnetic hydrogel was glued to a temperature sensor (DST nanoT, Star-Oddi) using cyanoacrylate adhesives (Loctite 460 instant adhesive). The temperature sensor had a size of 6 mm in diameter and 17 mm in length, completely encapsulated in the magnetic hydrogel. The sensor contained a tiny silver-oxide battery, which was weakly magnetic. The retention and localization of the integrated device in the artificial intestine were controlled by the external magnet. The presence of the external magnet did not influence the temperature readings of the sensor, and the presence of the sensor did not affect the magnetic retention (retention of a magnetic hydrogel alone in Figure S6b, Supporting Information; retention of a magnetic hydrogel and a temperature sensor in Figure 3g–i). 100 mL cold water ( $0\text{ }^{\circ}\text{C}$ ) was infused from the inlet of the phantom to replicate the water drinking. The temperature sensor was retrieved from the outlet of the phantom and the temperature over time was recorded at different spots in the phantom.

**Chemical Element Analysis in Leaching Solutions:** Leaching test of magnetic hydrogels was performed by incubating 1 g of the magnetic hydrogel in 1 mL of simulated intestinal fluid (pH 6.8)<sup>[13]</sup> for 0–10 days or 1 mL of simulated gastric fluid (pH 1.2)<sup>[13]</sup> for 0–1 day. Leached elements in the solutions were identified and quantified by inductively coupled plasma mass spectrometry (ICP-MS). ICP-MS analysis was performed on an Agilent 7900 instrument in helium mode ( $4.5\text{ mL min}^{-1}$  flow rate). 2%  $\text{HNO}_3$  was used as a rinse solution, and 10 ppb terbium was included as an internal standard among all samples. Calibration standards were prepared by volumetric dilution of a multielement standard. Both calibration standards and experimental samples were diluted with 2%  $\text{HNO}_3$  to ensure the stability of elements before spectroscopic analysis. Data were collected and analyzed for the following elements of interest:  $^{56}\text{Fe}$  and  $^{146}\text{Nd}$ .

**In Vitro Biocompatibility:** In vitro biocompatibility tests were conducted using a magnetic hydrogel-conditioned medium for Caco-2 (American Type Culture Collection) cell culture. There were no bacteria in the magnetic hydrogel for the biocompatibility test. To prepare the magnetic hydrogel-conditioned medium for in vitro cytotoxicity tests, 20 mg of the magnetic hydrogel was incubated in 1 mL of Dulbecco's modified Eagle medium (DMEM, Life Technologies) at  $37\text{ }^{\circ}\text{C}$  for 1, 4, 7 days. Caco-2 cells were cultured in DMEM supplemented with 10% fetal bovine serum (Sigma-Aldrich), 1 $\times$  non-essential amino acids solution (Life Technologies), 1 $\times$  GlutaMAX (Life Technologies), and penicillin/streptomycin (Life Technologies), and plated in 96-well plates. The cells were then treated with the magnetic hydrogel-conditioned medium and incubated at  $37\text{ }^{\circ}\text{C}$  for 48 h in 5%  $\text{CO}_2$ . Cells grown in pristine DMEM were used as a positive control. Cells grown in pristine DMEM and then treated with 70% ethanol for 30 min were used as a negative control. Cell viability was determined by using a live/dead viability/cytotoxicity kit for mammalian cells (Life Technologies). A confocal microscope (SP 8, Leica) was used to image live cells with excitation/emission at 495 nm/515 nm, and dead cells at 495 nm/635 nm. Live and dead cell numbers were counted using ImageJ, and the ratio of live cells to all cells in the images was calculated as Caco-2 cell viability.

**Bacterial Viability in Hydrogels:** 1 g of magnetic hydrogels containing living bacteria were incubated in 20 mL of fresh LB broth at 37 °C for 1–7 days, and the media were changed every 12 h. To test the bacterial viability, the hydrogels were first washed with 0.85% NaCl solution and then stained using the live/dead BacLight bacterial viability kit. 15 min after staining, fluorescent imaging of samples ( $n = 3$ ) was carried out using a confocal microscope (SP 8, Leica). Magnetic hydrogels treated with 70% ethanol for 1 h were used as a negative control. The occupied areas of green ( $S_g$ ) and red colonies ( $S_r$ ) in the images were obtained using ImageJ, and the bacterial viability equaled the viable populations over all populations, that is,  $\text{viability} = S_g / (S_g + S_r)$  in Figure 4e,f.

**In Vitro Blood Sensing in Hydrogels Containing Bacteria:** The heme-sensing ability of bacteria in the magnetic hydrogel was induced by the 0.1 vol% defibrinated horse blood (Hemostat) in the culture media and incubated with shaking at 37 °C for 24 h. Luminescence of hydrogels was visualized via a ChemiDoc Imaging System (Bio-Rad), with an exposure time of 60 s. To quantify the luminescence, 0.1 g of magnetic hydrogels were homogenized in 1 mL of PBS with a 4 mm stainless steel bead using a Tissuelyser II (Qiagen) at 30 Hz for 5 min. Samples were centrifuged at  $1000 \times g$  for 1 min to deposit large hydrogel debris. The supernatant was serially diluted in sterile PBS and spot plated on MacConkey agar supplemented with  $50 \mu\text{g mL}^{-1}$  kanamycin. Colonies (CFU) were enumerated following overnight incubation at 37 °C. On the other hand, the luminescence in hydrogel homogenate was measured in a BioTek Synergy H1 Hybrid Reader with an integration time of 1 s and a sensitivity of 150. The normalized luminescence of the magnetic hydrogel on different days was calculated as the ratio of the luminescence values (RLU/CFU; RLU, relative luminescence) of the magnetic hydrogel induced by 0.1 vol% blood to that of a non-induced magnetic hydrogel (a negative control) on the same day.

**Retention in Mouse Intestine:** All mouse experiments were approved by the Committee on Animal Care at the Massachusetts Institute of Technology (protocol number: 0818-075-21). Specific-pathogen free (SPF), male C57BL/6j mice (8–10 weeks of age) were purchased from Jackson Labs and were housed and handled under conventional conditions. Mice were acclimated to the animal facility 1 week prior to the commencement of experiments. Magnetic hydrogels containing engineered bacteria were prepared and incubated in fresh LB broth for 24 h. Then, the hydrogels were cut into small particles (radius 1 mm, thickness 1 mm) by a razor blade and dispersed in a block of nutritious jelly (DietGel 76A, ClearH<sub>2</sub>O). The nutritious jelly was provided to mice after overnight fasting. After mice ingested the jelly and magnetic hydrogels, X-ray microtomography (microCT, Bruker) was used to visualize the 3D spatial position of magnetic hydrogels in the GI tract over time. Mice with magnetic hydrogels inside their bodies are allocated into two groups: the control group without any treatment ( $n = 5$ ), while the experimental group carrying a disc-shaped magnet (D71-52, K&J Magnetics) adhered on the abdomen ( $n = 5$ ). The disc-shaped magnet was attached to the shaved abdomen skin and adhered by a layer of Histoacryl flexible adhesive (B. Braun Medical Inc.), and then mice were singly housed to prevent magnet-induced physical harm. The magnetic hydrogel retention in the mouse intestine was monitored by microCT in the experimental group daily for 7 days. All animals were monitored clinically at least twice a day for any evidence of morbidity, including lethargy, inappetence, decreased fecal output, abdominal distension, and decreased body weight.

**Blood Sensing in Mouse Intestine:** To examine the blood sensing ability of magnetic hydrogels in vivo, it was evaluated whether magnetic hydrogels containing engineered bacteria that retained in the intestine could detect upper GI bleeding elicited by oral indomethacin administration. Before indomethacin treatment, mice had taken the magnetic hydrogel containing bacteria and a small magnet disc was fixed on the abdomen skin. After 12-h retention of magnetic hydrogels in the intestine, GI bleeding was induced by indomethacin. Indomethacin (Sigma-Aldrich) solution was prepared by dissolving the compound in absolute ethanol to a concentration of  $20 \text{ mg mL}^{-1}$ . Immediately prior to mouse gavage, the indomethacin stock solution was diluted to  $2 \text{ mg mL}^{-1}$  in PBS, and the dilute indomethacin solution was administered to each animal in the treatment group ( $10 \text{ mg kg}^{-1}$ ). In the control group, mice

were fed with 0.2 mL of PBS. In the following morning, gastrointestinal bleeding was confirmed by performing a guaiac test (Hemoccult, Beckman Coulter) on fecal pellets from each animal. Magnet discs on the abdomen were removed and fecal pellets were collected at 1–6 h after magnet removal. The presence of magnetic hydrogels in the fecal pellets was checked by CT scanning of the collected fecal samples. The feces with magnetic hydrogels were used for luminescence analysis and CFU enumeration, and luminescence values were normalized to CFU values and reported in RLU/CFU.

**Histology Analysis:** All mice were sacrificed for histopathological analysis after experiments. Small intestines with and without the magnetic hydrogels were isolated, gently cleaned with PBS, fixed in 10% formaldehyde for 24 h, embedded in paraffin, sectioned, and stained with haematoxylin and eosin. Standard H&E-stained sections for the segments of interest were examined.

**Finite Element Simulations:** Three dimensional finite element model was built to simulate the stress distribution in the human intestine when a magnetic hydrogel was conformed to the human intestine. The geometries of the human intestine and magnetic hydrogel device were imported into ABAQUS CAE using STEP files generated from a commercial 3D modelling software. The imported geometry was subsequently meshed using eight-node brick elements with reduced integration (ABAQUS element type C3D8R) for both the human intestine and the magnetic hydrogel device. The normal pressure of 1 kPa was applied to the in-plane surface of the hydrogel. The boundary conditions and geometrical dimensions were summarized in Figure S2c, Supporting Information. To capture the non-linear elastic response of both the human intestine tissue<sup>[49]</sup> and magnetic hydrogel, incompressible Ogden model was adopted with the strain energy density of

$$W = \sum_{i=1}^N \frac{2\mu_i}{\alpha_i^2} (\bar{\lambda}_1^{\alpha_i} + \bar{\lambda}_2^{\alpha_i} + \bar{\lambda}_3^{\alpha_i} - 3) + \sum_{i=1}^N \frac{1}{D_i} (J-1)^{2i} \quad (3)$$

where  $\bar{\lambda}_i = J^{-1/3} \lambda_i$ , with  $J = \lambda_1 \lambda_2 \lambda_3$ ,  $\mu_i$  and  $\alpha_i$  represents material parameters fitted from the experimentally measured stress versus stretch curve,  $N$  represents the order parameter which is set as 1 here. By fitting with the model, the material parameters for the human intestine were identified as  $\mu_1 = 4.75 \text{ kPa}$  and  $\alpha_1 = 11.92$ , while that for the magnetic hydrogel were identified as  $\mu_1 = 4.38 \text{ kPa}$  and  $\alpha_1 = 3.23$  (Figure S2a,b, Supporting Information).  $D_1$  was set as 0.01 to impose the incompressible condition of the human intestine and the magnetic hydrogel disc.

**Data Analysis and Statistics:** All data were analyzed using Microsoft Excel and MATLAB (MathWorks). The computation of magnetic fields, forces, and pressures was implemented via MATLAB (MathWorks). As noted, error bars represent the standard deviation of at least three independent experiments. Significance between groups was determined using a two-sample, one-tailed Student's  $t$ -test assuming unequal variances.

**Code Availability:** Acquisition and analysis code will be available on reasonable request.

## Supporting Information

Supporting Information is available from the Wiley Online Library or from the author.

## Acknowledgements

X.L., Y.Y., and M.E.I. contributed equally to this work. The authors thank Tian Luo, Cheng Chang, Karen Pepper, Liu Wang, Sufeng Zhang, and Huanhuan Tian for helpful discussion; Mark Mimee for providing biosensor bacteria; and Milton Cornwall-Brady, Virginia Spanoudaki, David Bono, and Bogdan Fedeles for their training and assistance in operating the analytical instrumentations. This



work is supported by MIT, the US National Science Foundation (NSF; EFMA-1935291, CCF-1521925 and DMR-1419807), Defense Threat Reduction Agency (DTRA; E2045481 via George Mason University, HDTRA1-15-1-0050, and HDTRA1-14-1-0007), Leona M. and Harry B. Helmsley Charitable Trust (3239), National Institutes of Health (NIH; 229825 via Massachusetts General Hospital, 4-R33-A1121669-04, 1R01HL153857-01), U.S. Army Medical Research and Materiel Command (W81XWH-16-1-0565, W81XWH-17-1-0159, and W81XWH-18-1-0513), Space and Naval Warfare Systems Center (N66001-13-C-4025), Defense Advanced Research Projects Agency (DARPA; 152304.5106735.0006 and HR0011-15-C-0084), Army Research Office (W911NF-17-2-0077, W911NF-13-D-0001 T.O. 8), Human Frontier Science Program (LT000595/2017-L), Singapore-MIT Alliance for Research and Technology (S.M.A.R.T.), and Pew Charitable Trusts (to M.E. Inda; 00030623).

## Conflict of Interest

T.K.L. is a co-founder of Senti Biosciences, Synlogic, Engine Biosciences, Tango Therapeutics, Corvium, BiomX, Eligo Biosciences, Bota.Bio, Avendesora, and NE47Bio. TKL also holds financial interests in nest.bio, Armata, IndieBio, MedicusTek, Quark Biosciences, Personal Genomics, Thryve, Lexent Bio, MitoLab, Vulcan, Serotiny, Avendesora, Pulmobiotics, Provectus Algae, Invaio, and NSG Biolabs.

## Data Availability Statement

The main data supporting the findings of this study are available within the article and its Supporting Information. Additional data are available from the corresponding author upon reasonable request.

## Keywords

blood sensors, ingestible materials, intestinal retention, magnetic hydrogels, synthetic biology

Received: December 28, 2020

Revised: March 11, 2021

Published online:

- [1] D. T. Riglar, P. A. Silver, *Nat. Rev. Microbiol.* **2018**, *16*, 214.
- [2] C. Steiger, A. Abramson, P. Nadeau, A. P. Chandrakasan, R. Langer, G. Traverso, *Nat. Rev. Mater.* **2019**, *4*, 83.
- [3] K. Kalantar-Zadeh, K. J. Berean, N. Ha, A. F. Chrimes, K. Xu, D. Grando, J. Z. Ou, N. Pillai, J. L. Campbell, R. Brkljača, *Nat. Electron.* **2018**, *1*, 79.
- [4] D. T. Riglar, T. W. Giessen, M. Baym, S. J. Kerns, M. J. Niederhuber, R. T. Bronson, J. W. Kotula, G. K. Gerber, J. C. Way, P. A. Silver, *Nat. Biotechnol.* **2017**, *35*, 653.
- [5] B. Lim, M. Zimmermann, N. A. Barry, A. L. Goodman, *Cell* **2017**, *169*, 547.
- [6] J. M. Pickard, C. F. Maurice, M. A. Kinnebrew, M. C. Abt, D. Schenten, T. V. Golovkina, S. R. Bogatyrev, R. F. Ismagilov, E. G. Pamer, P. J. Turnbaugh, *Nature* **2014**, *514*, 638.
- [7] J. W. Kotula, S. J. Kerns, L. A. Shaket, L. Siraj, J. J. Collins, J. C. Way, P. A. Silver, *Proc. Natl. Acad. Sci. U. S. A.* **2014**, *111*, 4838.
- [8] M. Mimeo, R. J. Citorik, T. K. Lu, *Adv. Drug Delivery Rev.* **2016**, *105*, 44.
- [9] X. Liu, C. Steiger, S. Lin, G. A. Parada, J. Liu, H. F. Chan, H. Yuk, N. V. Phan, J. Collins, S. Tamang, G. Traverso, X. Zhao, *Nat. Commun.* **2019**, *10*, 493.
- [10] C. Hillemeier, *Pediatrics* **1995**, *96*, 997.
- [11] C. J. Bettinger, *Trends Biotechnol.* **2015**, *33*, 575.
- [12] M. Mimeo, P. Nadeau, A. Hayward, S. Carim, S. Flanagan, L. Jerger, J. Collins, S. McDonnell, R. Swartwout, R. J. Citorik, V. Bulović, R. Langer, G. Traverso, A. P. Chandrakasan, T. K. Lu, *Science* **2018**, *360*, 915.
- [13] S. Zhang, A. M. Bellinger, D. L. Gletting, R. Barman, Y.-A. L. Lee, J. Zhu, C. Cleveland, V. A. Montgomery, L. Gu, L. D. Nash, D. J. Maitland, R. Langer, G. Traverso, *Nat. Mater.* **2015**, *14*, 1065.
- [14] A. Abramson, E. Caffarel-Salvador, V. Soares, D. Minahan, R. Y. Tian, X. Lu, D. Dellal, Y. Gao, S. Kim, J. Wainer, J. Collins, S. Tamang, A. Hayward, T. Yoshitake, H.-C. Lee, J. Fujimoto, J. Fels, M. R. Frederiksen, U. Rahbek, N. Roxhed, R. Langer, G. Traverso, *Nat. Med.* **2019**, *25*, 1512.
- [15] S. C. Payne, J. B. Furness, M. J. Stebbing, *Nat. Rev. Gastroenterol. Hepatol.* **2019**, *16*, 89.
- [16] J.-M. Dumonceau, *Obes. Surg.* **2008**, *18*, 1611.
- [17] G. M. Cobrin, M. T. Abreu, *Immunol. Rev.* **2005**, *206*, 277.
- [18] B. P. Landry, J. J. Tabor, in *Bugs as Drugs: Therapeutic Microbes for the Prevention and Treatment of Disease* (Eds.: R. A. Britton, P. D. Cani), Wiley, Hoboken, NJ **2018**, Ch. 14.
- [19] A. J. Moës, *Crit. Rev. Ther. Drug.* **1993**, *10*, 143.
- [20] S.-J. Hwang, H. Park, K. Park, *Crit. Rev. Ther. Drug.* **1998**, *15*, 243.
- [21] A. H. Sarmast, H. I. Showkat, A. M. Patloo, F. Q. Parray, R. Lone, K. A. Wani, *Br. J. Med. Pract.* **2012**, *5*, A529.
- [22] J.-S. Park, S. Jeong, D. H. Lee, *Clin. Endosc.* **2015**, *48*, 209.
- [23] J. D. Smart, *Adv. Drug Delivery Rev.* **2005**, *57*, 1556.
- [24] S. Y. Yang, E. D. O’Cearbhaill, G. C. Sisk, K. M. Park, W. K. Cho, M. Villiger, B. E. Bouma, B. Pomahac, J. M. Karp, *Nat. Commun.* **2013**, *4*, 1702.
- [25] Y. Lee, T. E. Deelman, K. Chen, D. S. Y. Lin, A. Tavakkoli, J. M. Karp, *Nat. Mater.* **2018**, *17*, 834.
- [26] P. Praveschotinunt, A. M. Duraj-Thatte, I. Gelfat, F. Bahl, D. B. Chou, N. S. Joshi, *Nat. Commun.* **2019**, *10*, 5580.
- [27] Y. Kim, H. Yuk, R. Zhao, S. A. Chester, X. Zhao, *Nature* **2018**, *558*, 274.
- [28] Y. Kim, G. A. Parada, S. Liu, X. Zhao, *Sci. Robot.* **2019**, *4*, eaax7329.
- [29] K. T. Gottlieb, S. Banerjee, B. A. Barth, Y. M. Bhat, S. S. Chauhan, V. Konda, J. T. Maple, F. Murad, P. Pfau, D. Pleskow, *Gastrointest. Endosc.* **2013**, *78*, 561.
- [30] Z. Wu, L. Li, Y. Yang, P. Hu, Y. Li, S.-Y. Yang, L. V. Wang, W. Gao, *Sci. Robot.* **2019**, *4*, eaax0613.
- [31] S. Gabriel, R. Ackermann, *JPEN, J. Parenter. Enteral Nutr.* **2004**, *28*, 119.
- [32] B. Laulicht, N. J. Gidmark, A. Tripathi, E. Mathiowitz, *Proc. Natl. Acad. Sci. U. S. A.* **2011**, *108*, 2252.
- [33] S. Yim, E. Gultepe, D. H. Gracias, M. Sitti, *IEEE. Trans. Biomed. Eng.* **2014**, *61*, 513.
- [34] C. Hu, M. Q. H. Meng, M. Mandal, *Int. J. Inf. Acquis.* **2005**, *02*, 23.
- [35] S. Lin, J. Liu, X. Liu, X. Zhao, *Proc. Natl. Acad. Sci. U. S. A.* **2019**, *116*, 10244.
- [36] S. Lin, X. Liu, J. Liu, H. Yuk, H.-C. Loh, G. A. Parada, C. Settens, J. Song, A. Masic, G. H. McKinley, *Sci. Adv.* **2019**, *5*, eaau8528.
- [37] K&J Magnetics, Inc., Demagnetization (BH) Curves for Neodymium Magnets, <https://www.kjmagnetics.com/bhcurves.asp> (accessed: June 2020).
- [38] R. K. Avvari, in *Digestive System-Recent Advances*, IntechOpen, London, UK **2019**.
- [39] Y. Sambuy, I. De Angelis, G. Ranaldi, M. L. Scarino, A. Stamatii, F. Zucco, *Cell Biol. Toxicol.* **2005**, *21*, 1.
- [40] X. Liu, H. Yuk, S. Lin, G. A. Parada, T.-C. Tang, E. Tham, C. de la Fuente-Nunez, T. K. Lu, X. Zhao, *Adv. Mater.* **2018**, *30*, 1704821.
- [41] X. Liu, T.-C. Tang, E. Tham, H. Yuk, S. Lin, T. K. Lu, X. Zhao, *Proc. Natl. Acad. Sci. U. S. A.* **2017**, *114*, 2200.
- [42] T. L. A. Nguyen, S. Vieira-Silva, A. Liston, J. Raes, *Dis. Models Mech.* **2015**, *8*, 1.
- [43] F. Hugenholtz, W. M. de Vos, *Cell. Mol. Life Sci.* **2018**, *75*, 149.

- [44] V. M. Isabella, B. N. Ha, M. J. Castillo, D. J. Lubkowitz, S. E. Rowe, Y. A. Millet, C. L. Anderson, N. Li, A. B. Fisher, K. A. West, P. J. Reeder, M. M. Momin, C. G. Bergeron, S. E. Guilmain, P. F. Miller, C. B. Kurtz, D. Falb, *Nat. Biotechnol.* **2018**, *36*, 857.
- [45] M. E. Sanders, D. J. Merenstein, G. Reid, G. R. Gibson, R. A. Rastall, *Nat. Rev. Gastroenterol. Hepatol.* **2019**, *16*, 605.
- [46] Z. Z. R. Hamady, N. Scott, M. D. Farrar, J. P. A. Lodge, K. T. Holland, T. Whitehead, S. R. Carding, *Gut* **2010**, *59*, 461.
- [47] L. Steidler, W. Hans, L. Schotte, S. Neiryck, F. Obermeier, W. Falk, W. Fiers, E. Remaut, *Science* **2000**, *289*, 1352.
- [48] G. A. Parada, H. Yuk, X. Liu, A. J. Hsieh, X. Zhao, *Adv. Healthcare Mater.* **2017**, *6*, 1700520.
- [49] M. B. Christensen, K. Oberg, J. C. Wolchok, *SpringerPlus* **2015**, *4*, 142.